Extreme Mechanics Letters 12 (2017) 48–54

Contents lists available at ScienceDirect

Extreme Mechanics Letters

journal homepage: www.elsevier.com/locate/eml

Enhanced acoustic insulation properties of composite metamaterials having embedded negative stiffness inclusions

D. Chronopoulos [a,*], I. Antoniadis [b], T. Ampatzidis [a]

[a] Institute for Aerospace Technology & The Composites Group, The University of Nottingham, NG7 2RD, UK

[b] Machine Design and Control Systems Section, School of Mechanical Engineering, National Technical University of Athens, Greece

ARTICLE INFO

Article history:
Received 27 February 2016
Received in revised form
12 September 2016
Accepted 12 October 2016
Available online 19 November 2016

Keywords:
Mechanical metamaterials
Wave propagation
Negative stiffness
Composite structures
Damping

ABSTRACT

Despite the fact that the concept of incorporating Negative Stiffness (NS) elements within mechanical systems was formulated and validated more than 40 years ago, it has only recently received consistent attention. In this work, the design of a layered mechanical metamaterial having implemented NS inclusions is presented and its acoustic wave propagation properties are modelled. A dedicated two-dimensional periodic structure theory scheme is developed in order to compute the frequency dependent damping loss factor of the metamaterial structure. The acoustic transmission properties through the modelled panel are computed within a Statistical Energy Analysis (SEA) scheme. It is demonstrated that the suggested layered metamaterial exhibits highly superior acoustic insulation performance close and above the acoustic coincidence range, thanks to the drastic increase of its structural damping properties implied by the NS elements. Additionally, the proposed configuration presents superior performance in a broadband frequency range when compared to a viscoelastic damping constraint layer of equivalent mass.

1. Introduction

The need for low-cost and low-mass vibration isolation within the modern aerospace, automotive and energy industries has recently motivated research groups at a worldwide level to develop a number of novel vibration isolation concepts. Moreover, the use of composite layered materials in the transport industry is becoming more important due to the need for designing and manufacturing lightweight, energy efficient products. Despite their superior structural characteristics, composite structures exhibit inferior dynamic and acoustic performance levels compared to conventional metallic ones. The large number and variety of elastic waves propagating within a layered composite, implies high structure-borne vibration transmissibility and high noise transmission. Structural integrity as well as passenger comfort can be compromised by high levels of vibration and noise transmitted through industrial structures. Widely employed damping enhancement methodologies nowadays include the addition of viscoelastic material layers that are expensive in terms of additional, non-structural mass and space usage. Moreover, it is also noted that whilst viscoelastics have shown potential for increasing attenuation in the high frequency domain, there is currently no recognised passive design configuration for efficiently damping low frequency vibration (that is the first 5–10 structural modes). Research interest has therefore focused towards achieving increased structural damping through measures of reduced mass, volume and cost impact. A methodology receiving increasing attention due to its attenuation efficiency (particularly in the low-frequency range) is the inclusion of internal tuned resonators [1]. As demonstrated below, a number of authors has suggested that the inclusion of negative stiffness elements in the structural ensemble, can drastically amplify internal oscillations and consequently the structural damping performance of the configuration.

The beneficial impact of NS mechanisms on vibration isolation has been reported as early as 1957 in the pioneering publication of Molyneaux [2]. It was followed by the milestone developments of the authors in [3,4] where the design of mechanical isolating NS mechanisms was achieved through the use of discrete macroscopic elements. It was demonstrated that the exceptional performance of these systems was attained through reducing the strain energy stored within the system during oscillation (by reduction of the overall effective stiffness), thus increasing the loss factor of the

* Corresponding author.
E-mail address: Dimitrios.Chronopoulos@nottingham.ac.uk (D. Chronopoulos).

http://dx.doi.org/10.1016/j.eml.2016.10.012
2352-4316/

oscillator defined as:

$$\eta = \frac{\text{energy dissipated per cycle}}{\text{maximum strain energy stored in the system}}. \quad (1)$$

There exist generally two design streams of NS inspired structures; one of them focusing on the development of continuous metamaterials containing NS phase inclusions (see [5]) and the second one dedicated to the design of systems containing discrete macroscopic NS elements. Both research streams share common reported benefits (high structural damping and vibration isolation performance levels) however not the same challenges. With regard to the design of macroscopic NS elements, a variety of designs has been proposed for the realisation of such configurations, incorporating various structural elements such as post-buckled beams, plates, shells and precompressed springs, arranged in appropriate geometrical configurations [6–11]. Experimental validation of NS vibration isolation mechanisms with their designs based on Euler post-buckled beams have been presented in [12–16]. In automotive engineering, applications include the design of NS suspensions [17,18] as well as vibration isolation seats [19–21] for improved passenger comfort. A high-speed railroad vibration isolation system employing NS elements was discussed in [22]. The authors in [23–26], employed structural NS elements at the basis of civil structures in order to suppress vibration without large force transmission to the superstructure during extreme earthquake excitations.

Multiphysics NS mechanisms incorporating magnetic and magnetorheological fluid elements have been proposed, however the additional mass required by such designs prohibits their application in moving structures. In [27–29] a NS magnetic spring mechanism exhibited high vibration isolation performance levels. In [30,31] the authors suggested magnetorheological adjustable NS devices with enhanced vibration isolation properties. In [32] the design principles and experimental validation of magnetic NS dampers were presented, comprising several permanent magnets in a conductive pipe.

In this paper the authors propose the design of a novel layered mechanical metamaterial having implemented NS inclusions. The design and tailoring of the mechanical characteristics of the internal NS inclusions is initially discussed. A two-dimensional periodic structure theory scheme is employed and modified in order to derive a dedicated expression for the damping loss factor of the structure as a function of the elastic waves propagating within it. The acoustic transmission properties through the modelled panel are computed within a statistical energy analysis scheme. The numerical results provide evidence of a drastic increase of the damping loss factor as well as of the acoustic isolation performance of the proposed NS layered metamaterial in a broadband frequency range.

The paper is organised as follows: In Section 2 the design of the mechanical NS inclusions is discussed and a number of numerical parametric results are provided on a variety of NS designs. In Section 3 a periodic layered structure having NS inclusions is Finite Element (FE) modelled. The characteristics of the elastic waves propagating within the structure are sought through a two-dimensional periodic structure theory scheme. The damping loss factor associated with each propagating wave type is computed, as is the sound Transmission Loss (TL) of the structural panel. Conclusions on the exhibited work are eventually drawn in Section 4.

2. Design of mechanical NS internal inclusions

In this work, the authors are interested in implementing macroscopic NS elements with mechanical characteristics specifically tailored for maximising the damping properties of the considered layered composite structure. As weight is a design factor of principal importance, configurations of a purely mechanical nature will be preferred. The majority of mechanical NS designs proposed by researchers nowadays are generally related to Euler beams operating in their post-buckling regime. Such structures are straightforward to manufacture and incorporate, however in the case of being implemented within the honeycomb core of a layered structure they could induce highly asymmetric stress loading conditions within the structural core, leading to possible fatigue and failure.

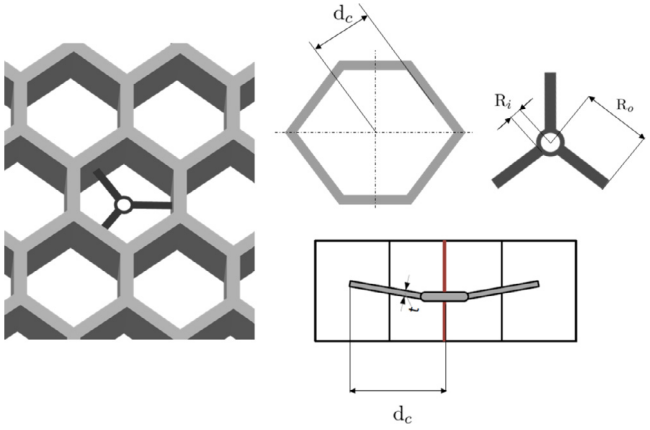

Fig. 1. Illustration of the proposed tripod mechanism: Left: View of the employed prestressed NS elements within the honeycomb architecture of the core structure. Right: Side view of the NS elements within a honeycomb cell. Positive stiffness elements and honeycomb cell are also illustrated.

In this work, an element that is more stable and suitable for implementation in honeycomb cores is proposed as illustrated in Fig. 1. Similar to a beam, the proposed tripod structure snaps through around the equilibrium point during operation, rendering it effectively a NS element around that region. Positive stiffness (viscoelastic straps) are attached to the element in order to render the ensemble of the inclusion stable, and facilitate its activation during operation.

A parametric survey is hereby performed in order to determine the sensitivity of the NS characteristics of the proposed structure as a function of its design. For this reason, the inclusion is FE modelled as illustrated in Fig. 2 and nonlinear quasi-static solutions are sought in order to determine its mechanical characteristics within the operational displacement regime. The stress distribution on the honeycomb cell was tested as shown in Fig. 3 and proved to be satisfactory. More specifically, using technical characteristics of honeycomb that is commercially available, the FE analysis showed that the stresses that were applied on the honeycomb cell during the snapping movement of the tripod mechanism did not exceed the 10% of the material's strength. The design characteristics under investigation are the ratio of the mechanism's outer and inner dimensions $r_R = R_o/R_i$, the thickness t as well as the prestress factor equal to the ratio of the outer dimension of the mechanism R_o and the actual size of the honeycomb cell d_c expressed as $p_f = R_o/d_c$. A two-step, nonlinear quasi-static analysis is performed. The structure is initially prestressed to the position corresponding to it being fitted inside the honeycomb cell. A small perturbation load is applied in order to facilitate the convergence of the FE solution close to the bifurcation point of the analysis (i.e. ensure a stable deflection of the tripod structure upwards during precompression). The second step consists in applying displacement constraints at the central ring of the tripod in order to trigger the snap-through process. The reaction forces measured at the supports are exhibited below.

The general trend for the displacement/force characteristics of the snap-through region of the proposed configuration are shown in Fig. 4. It is observed that a lower r_R factor will not only imply

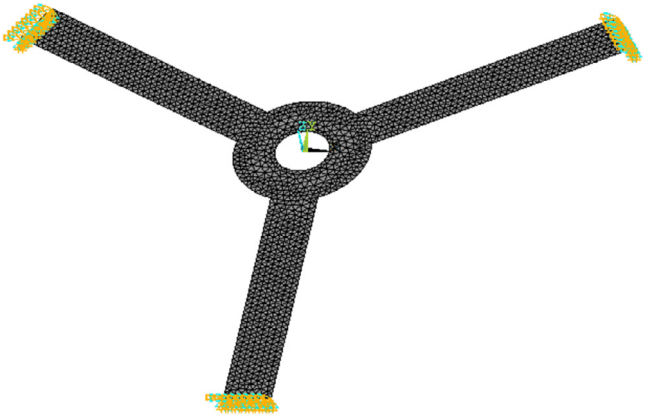

Fig. 2. Caption of the FE model employed for the quasi-static analysis of the tripod mechanism.

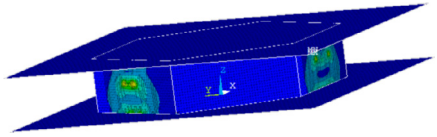

Fig. 3. Caption of the stress distribution of the FE model during the snapping movement of the tripod mechanism embedded in the hexagon cell of the honeycomb.

Table 1
Dimensions of the tripod mechanism of the parametric survey. Thickness of the tripod was the same for all the cases ($t = 0.5$ mm).

	$p_f = 1.2$		
$r_R = 10/8$	$R_o = 10$ mm	$R_i = 8$ mm	$d_c = 8.3$ mm
$r_R = 10/4$	$R_o = 10$ mm	$R_i = 4$ mm	$d_c = 8.3$ mm
$r_R = 10/2$	$R_o = 10$ mm	$R_i = 2$ mm	$d_c = 8.3$ mm
	$r_R = 10/8$		
$p_f = 1.2$	$R_o = 20$ mm	$R_i = 16$ mm	$d_c = 16.7$ mm
$p_f = 1.1$	$R_o = 20$ mm	$R_i = 16$ mm	$d_c = 18.2$ mm
$p_f = 1.05$	$R_o = 20$ mm	$R_i = 16$ mm	$d_c = 19$ mm

reduced weight for the device but it will also result in a more pronounced NS region and a higher NS coefficient. For higher r_R factors the NS region of the displacement/force characteristics tends to be minimised. A parametric study on the influence of the p_f design parameter on the snap-through characteristics of the device are presented in Fig. 5. It is observed that employing a higher prestress factor leads to a more intense NS behaviour (as intuitively expected). The same choice leads to a longer NS operation region for the device which is also beneficial for maximising internal energy absorption. It is noted that the curves in Fig. 5 are interrupted just after the snap-through movement of the oscillator is completed (the displacement/force characteristics will evidently enter an intense positive stiffness behaviour after that). Last but not least it is important to investigate the impact of the cell/tripod interface boundary conditions on the snap-through behaviour of the device. From the results exhibited in Fig. 6 it is evident that when the device is clamped on the honeycomb cell walls (that is any rotation is constrained at the interface nodes) the NS performance of the device is heavily compromised. Instead, the restriction on the orientation of the interface nodes implied a pronounces increase of the positive stiffness behaviour of the device (see Table 1).

In short, it can be concluded that an increase of the p_f design factor as well as a decrease of r_R can be beneficial for extending the NS region of the proposed device. Both design parameters can be employed for tailoring the NS constant of

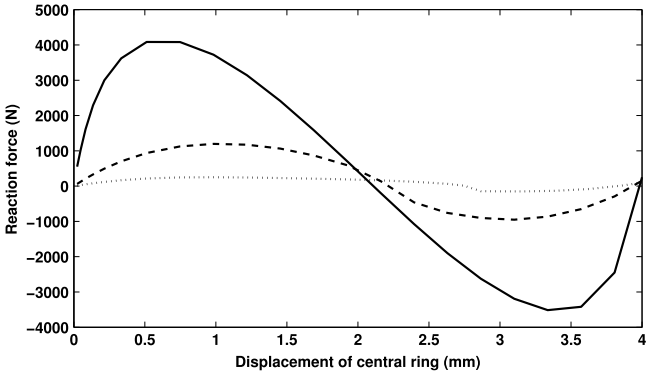

Fig. 4. Impact of the r_R design parameter on the snap-through characteristics of the proposed tripod mechanism. Displacement/force results for: $r_R = 10/8$ (–), $r_R = 10/4$ (- -), $r_R = 10/2$ (· · ·). All results are for $p_f = 1.2$.

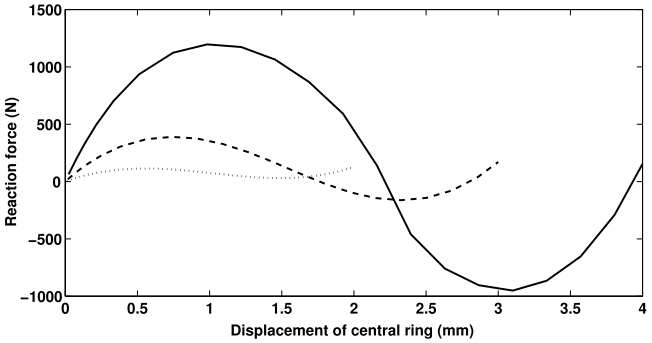

Fig. 5. Impact of the p_f design parameter on the snap-through characteristics of the proposed tripod mechanism. Displacement/force results for: $p_f = 1.2$ (–), $p_f = 1.1$ (- -), $p_f = 1.05$ (· · ·). All results are for $r_R = 10/8$.

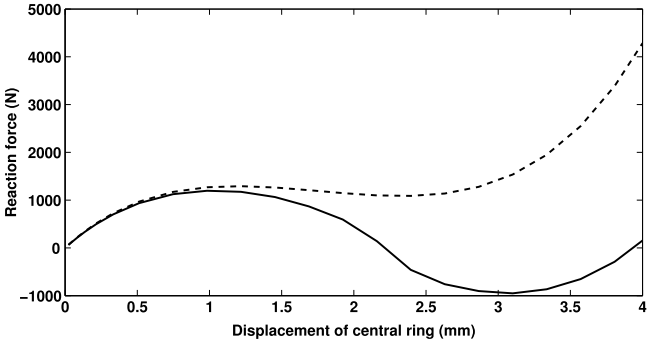

Fig. 6. Impact of the interface boundary conditions on the snap-through characteristics of the proposed tripod mechanism. Displacement/force results for: Simply supported boundary conditions (–) and clamped boundary conditions (- -). All results are for $r_R = 10/8$ and $p_f = 1.2$.

the designed device. Caution should be exercised when selecting the implementation process of the inclusion, as restricting the rotation DoF at the interface of the device can be detrimental for its NS characteristics. As exhibited by the above results, the displacement/force characteristics of the mechanisms can be approximated as linear around their snap-through position. A constant stiffness assumption will therefore be adopted in the following section.

3. Sound transmission through a layered metamaterial having NS inclusions

The configuration to be considered is a layered structural panel comprising two facesheets and a core layer (see Fig. 7). In order to

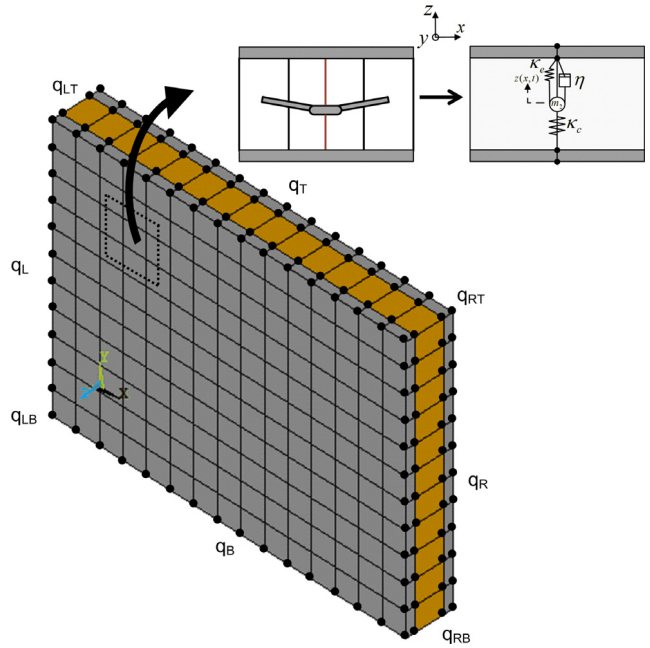

Fig. 7. Caption of the FE modelled composite layered panel with the interface edge and the interface corner DoF highlighted. The envisaged internal configuration of the inclusion, as well as the equivalent periodic structure (with m_2 the device's mass, κ_e the positive stiffness and κ_c the NS) are also illustrated.

account for the impact of the core shear deformation on the elastic wave propagation characteristics, a 3D displacement field will be assumed and the panel will be modelled by FE. An illustration of the internal tripod devices as well as the equivalent modelled periodic structural segment are also exhibited in the same figure. NS and positive stiffness elements are modelled as translational spring FEs connected to mass m_2 (representing the mass of the added NS mechanism). It is noted that the static and dynamic stability of the internal oscillator has been discussed in [33]. It is noted that the NS inclusions are assumed to have the same periodicity in the x and y directions.

In the following numerical case study, the metamaterial facesheets are assumed to have a Young's modulus $E_f = 70$ GPa, a Poisson's ratio $\upsilon_f = 0.3$ and a mass density of $\rho_f = 3000$ kg/m^3. The thickness of the facesheets is equal to $h_f = 1$ mm. The core has a thickness equal to $h_c = 6$ mm and is made of a material having $E_c = 0.7$ GPa, $\upsilon_c = 0.2$ and $\rho_c = 50$ kg/m^3. A constant damping loss factor $\eta_f = \eta_c = 1\%$ is assumed for both materials. The dimensions of the two-dimensional modelled periodic segment are $l_x = l_y = 50$ mm while the total dimensions of the panel L_x, L_y are equal to 1.5 m $\times$ 2 m. With regard to the NS inclusions design, added mass m_2 is assumed to be equal to 5% of the total mass of the panel. Out of the entirety of the investigated device configurations (as described in Section 2) it has been found that a NS device of $\kappa_c = -10$ kN/m combined with a positive stiffness one of $\kappa_e = 11$ kN/m will provide maximum structural damping enhancement.

3.1. Wave propagation and dissipation within the mechanical metamaterial

The mass, damping and stiffness matrices of the periodic segment $\mathbb{M}$, $\mathbb{C}$ and $\mathbb{K}$ are extracted using a conventional FE software. Time harmonic wave propagation is hereby considered within the layered structure in the x and y directions implying

$$z(x, y, \omega, t) = Z\mathrm{e}^{\mathrm{i}(\omega t - k_x x - k_y y)} \tag{2}$$

with $k_x = k\cos(\theta)$ and $k_y = k\sin(\theta)$ where k the propagating structural elastic wavenumber and θ the propagation direction. The problem will be modelled by a wave and finite element approach (coupling FE to periodic structure theory) similar to the one exhibited in [34]. The DoF set $\mathbf{q}$ (as well as the $\mathbb{M}, \mathbb{C}, \mathbb{K}$ matrices) is reordered according to a predefined sequence such as:

$$\mathbf{q} = \left\{\mathbf{q_I} \quad \mathbf{q_B} \quad \mathbf{q_T} \quad \mathbf{q_L} \quad \mathbf{q_R} \quad \mathbf{q_{LB}} \quad \mathbf{q_{RB}} \quad \mathbf{q_{LT}} \quad \mathbf{q_{RT}}\right\}^\top \tag{3}$$

corresponding to the internal, the interface edge and the interface corner DoF (see Fig. 7). The free harmonic vibration equation of motion for the modelled segment is written as:

$$[\mathbb{K} + \mathrm{i}\omega\mathbb{C} - \omega^2\mathbb{M}]\mathbf{q} = \mathbf{0}. \tag{4}$$

The following relations being assumed for the displacement DoF under the passage of a time-harmonic wave:

$$\begin{aligned} &\mathbf{q_R} = e^{-i\varepsilon_x}\mathbf{q_L}, \qquad \mathbf{q_T} = e^{-i\varepsilon_y}\mathbf{q_B} \\ &\mathbf{q_{RB}} = e^{-i\varepsilon_x}\mathbf{q_{LB}}, \qquad \mathbf{q_{LT}} = e^{-i\varepsilon_y}\mathbf{q_{LB}}, \qquad \mathbf{q_{RT}} = e^{-i\varepsilon_x - i\varepsilon_y}\mathbf{q_{LB}} \end{aligned} \tag{5}$$

with ε_x and ε_y the propagation constants in the x and y directions related to the phase difference between the sets of DoF. The wavenumbers k_x, k_y are directly related to the propagation constants through the relation:

$$\varepsilon_x = k_x L_x, \qquad \varepsilon_y = k_y L_y. \tag{6}$$

Considering Eq. (5) in tensorial form gives:

$$\mathbf{q} = \begin{bmatrix} \mathbf{I} & \mathbf{0} & \mathbf{0} & \mathbf{0} \\ \mathbf{0} & \mathbf{I} & \mathbf{0} & \mathbf{0} \\ \mathbf{0} & \mathbf{I}e^{-i\varepsilon_y} & \mathbf{0} & \mathbf{0} \\ \mathbf{0} & \mathbf{0} & \mathbf{I} & \mathbf{0} \\ \mathbf{0} & \mathbf{0} & \mathbf{I}e^{-i\varepsilon_x} & \mathbf{0} \\ \mathbf{0} & \mathbf{0} & \mathbf{0} & \mathbf{I} \\ \mathbf{0} & \mathbf{0} & \mathbf{0} & \mathbf{I}e^{-i\varepsilon_x} \\ \mathbf{0} & \mathbf{0} & \mathbf{0} & \mathbf{I}e^{-i\varepsilon_y} \\ \mathbf{0} & \mathbf{0} & \mathbf{0} & \mathbf{I}e^{-i\varepsilon_x - i\varepsilon_y} \end{bmatrix} \mathbf{x} = \mathbf{R}\mathbf{x} \tag{7}$$

with $\mathbf{x}$ the reduced set of DoF: $\mathbf{x} = \left\{\mathbf{q_I} \quad \mathbf{q_B} \quad \mathbf{q_L} \quad \mathbf{q_{LB}}\right\}^\top$. A number of numerical schemes can be employed in order to compute the solution of eigenvalue problems with frequency dependent matrices. However, at this point it is rational to assume that damping will have negligible impact on the real part of the propagating wavenumbers, (see [35,36]) in which case the equation of free harmonic vibration of the modelled segment can be written as:

$$[\mathbf{R}^*\mathbb{K}\mathbf{R} - \omega^2\mathbf{R}^*\mathbb{M}\mathbf{R}]\mathbf{x} = \mathbf{0} \tag{8}$$

with * denoting the Hermitian transpose. The most practical procedure for extracting the wave propagation characteristics of the segment from Eq. (8) is injecting a set of assumed propagation constants $\varepsilon_x, \varepsilon_y$. The set of these constants can be chosen in relation to the direction of propagation towards which the wavenumbers are to be sought and according to the desired resolution of the wavenumber curves. Eq. (8) is then transformed into a standard eigenvalue problem and can be solved for the eigenvector $\mathbf{x}_w$ which describe the deformation of the segment under the passage of each wave type w at an angular frequency equal to the square root of the corresponding eigenvalue $\lambda_w = \omega_w^2$. A complete description of each passing wave including its x and y directional wavenumbers and its wave shape for a certain frequency is therefore acquired. It is noted that the periodicity condition is defined modulo 2π, therefore solving Eq. (8) with a set of $\varepsilon_x, \varepsilon_y$ varying from 0 to 2π will suffice for capturing the entirety of the structural elastic waves. Further considerations on reducing the computational expense of the problem are discussed in [37].

3.1.1. Damping loss factor calculation

Within a vibroacoustic analysis it is valuable to compute and employ the damping loss factor of the entire panel $\eta_{w,\theta}$ when excited by a certain wave type w propagating towards direction θ at an angular frequency ω. The loss factor associated with a given propagating wave is defined as

$$\eta_{w,\theta}(\omega,\theta)=\frac{P_{diss,w}}{\omega(U_w+T_w)} \tag{9}$$

with P_{diss} the time-average power dissipated by structural damping, U the time-average strain energy and T the time-average kinetic energy in the modelled structural segment. By employing the appropriately normalised computed displacements $\mathbf{x}$ as derived by the eigenproblem in Eq. (8) the above quantities can be expressed as

$$\begin{aligned} T_w &= \frac{\omega^2}{2}\mathrm{Re}\left(\{\mathbf{q}_{w,\theta}\}^{\mathrm{H}}\mathbf{M}\{\mathbf{q}_{w,\theta}\}\right)\\ U_w &= \frac{1}{2}\mathrm{Re}\left(\{\mathbf{q}_{w,\theta}\}^{\mathrm{H}}\mathbf{K}\{\mathbf{q}_{w,\theta}\}\right)\\ P_{diss,w} &= \sum_n 2\omega\eta_n U_{n,w}\\ &= \omega\sum_n \mathrm{Re}\left(\{\mathbf{q}_{n,w,\theta}\}^{\mathrm{H}}\eta_n\mathbf{K}_n\{\mathbf{q}_{n,w,\theta}\}\right)\\ &= \omega^2\mathrm{Re}\left(\{\mathbf{q}_{w,\theta}\}^{\mathrm{H}}\mathbf{C}\{\mathbf{q}_{w,\theta}\}\right) \end{aligned} \tag{10}$$

with n the number of structural layers, η_n the damping loss factor of layer n and

$$\mathbf{q}_{w,\theta}=\begin{Bmatrix}\mathbf{q}_{I,w}\\ \mathbf{q}_{B,w}\\ \mathrm{e}^{-\mathrm{i}\varepsilon_y}\mathbf{q}_{B,w}\\ \mathbf{q}_{L,w}\\ \mathrm{e}^{-\mathrm{i}\varepsilon_x}\mathbf{q}_{L,w}\\ \mathbf{q}_{LB,w}\\ \mathrm{e}^{-\mathrm{i}\varepsilon_x}\mathbf{q}_{LB,w}\\ \mathrm{e}^{-\mathrm{i}\varepsilon_y}\mathbf{q}_{LB,w}\\ \mathrm{e}^{-\mathrm{i}\varepsilon_x-\mathrm{i}\varepsilon_y}\mathbf{q}_{LB,w}\end{Bmatrix} \tag{11}$$

being the displacements induced in the modelled segment by the propagating wave type w travelling in direction θ. By substituting Eq. (10) in Eq. (9) the general expression for the direction dependent damping loss factor $\eta_{w,\theta}$ is derived as

$$\eta_{w,\theta}=\frac{2\omega\mathrm{Re}\left(\{\mathbf{q}_{w,\theta}\}^{\mathrm{H}}\mathbf{C}\{\mathbf{q}_{w,\theta}\}\right)}{\mathrm{Re}\left(\{\mathbf{q}_{w,\theta}\}^{\mathrm{H}}\mathbf{K}\{\mathbf{q}_{w,\theta}\}\right)+\omega^2\mathrm{Re}\left(\{\mathbf{q}_{w,\theta}\}^{\mathrm{H}}\mathbf{M}\{\mathbf{q}_{w,\theta}\}\right)}. \tag{12}$$

Eventually, the global frequency dependent damping loss factor corresponding to wave type w can be computed as

$$\eta_w(\omega)=\frac{\int_0^{\pi}\eta_{w,\theta}(\omega,\theta)\mathrm{d}\theta}{\int_0^{\pi}\mathrm{d}\theta}. \tag{13}$$

The wave type transferring the dominant portion of energy during elasto-acoustic transmission will be the out-of-plane bending waves propagating through the structure. Following the wave propagation analysis, the frequency dependent damping loss factor for the bare panel (no inclusions) as well as for the modified panel incorporating NS elements has been computed and is presented in Fig. 8. As expected, the bare panel exhibits a constant damping behaviour with a loss factor equal to the one of the constituting materials, i.e. 1%. On the other hand, the results for two composite metamaterial panels are exhibited (with a 30 mm and a 50 mm periodicity respectively) both presenting an intensely frequency dependent loss factor. It becomes evident that the inclusion of the NS elements has a major impact in the low frequency range (η approximately two orders of magnitude higher), where the oscillation of the internal masses has a higher vibration amplitude. This is a major advantage compared to viscoelastic materials which start providing damping enhancement mainly in the high frequency range. The impact of the NS inclusions is gradually diminishing in the higher frequency range of the vibroacoustic analysis, with the benefits however still visible at 12 kHz, where the modified panel has a loss factor more than three times higher. It can be observed that increasing the periodicity of the internal oscillators has a negative impact on the panel's global damping ratio. In this case study a maximum loss of damping of approximately 32% was observed at very low frequencies (100 Hz).

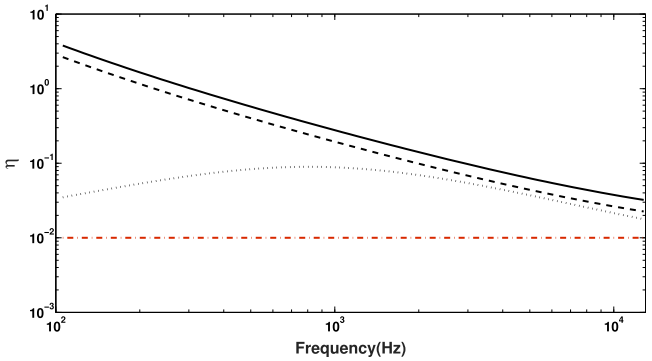

Fig. 8. Frequency dependent damping loss factor associated with the out-of-plane flexural wave for the layered metamaterial: Reference bare layered panel (---), metamaterial with NS inclusions having a 30 mm periodicity (–), metamaterial with NS inclusions having a 50 mm periodicity (- -), panel with a mass-equivalent polyvinyl butyral (PVB) layer inclusion (· · ·).

As aforementioned, the principal advantage of the suggested configuration over viscoelastic materials is that the latter tend to provide significant damping enhancement only in the high frequency range. In order to verify this advantage, an additional result is presented in Fig. 8 where a constrained damping layer of polyvinyl butyral (PVB) is added between the core and the upper facesheet of the structure. PVB is considered amongst the most efficient viscoelastic additions in the industry with a damping loss factor of $\eta_d = 40\%$. In order for the investigated models to be equivalent, the added PVB layer will also account for 5% of the bare panel's mass (same as for the metamaterial having a 30 mm periodicity). This corresponds to a PVB layer thickness of $h_d = 0.47$ mm. The constrained damping layer has $E_d = 10$ MPa, $\rho_d = 1000$ kg/m^3 and $\upsilon_d = 0.48$. It can be observed that in the low frequency range the damping implied by the constrained layer is approximately 90 times inferior to the one of the equivalent NS metamaterial. It is only after 3 kHz that the damping induced by the constrained layer becomes comparable to the metamaterial one. It is also worth noting that even in the very high frequency range, the NS oscillators will provide similar damping enhancement to the constrained damping layer.

3.2. Calculation of the acoustic transmission through the panel

It is now of interest to investigate how the enhanced damping properties of the composite metamaterial can impact its noise insulation properties. For this reason a wave-based statistical energy analysis scheme as exhibited in [37,38] is employed, in which the computed wavenumber and damping loss factor values for the panel are input. The major vibroacoustic index that provides an important indication of a structure's acoustic opacity properties is its sound TL. The TL indices for the bare composite, as well as for the layered metamaterial are presented in Fig. 9.

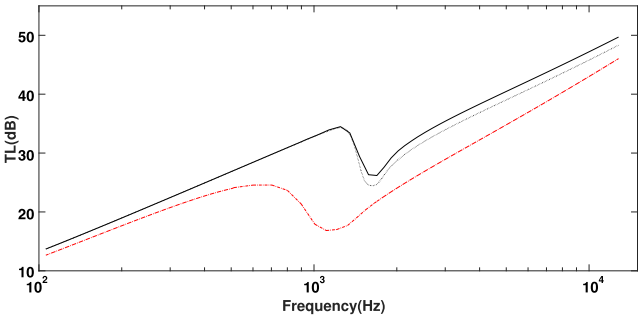

Fig. 9. Broadband sound Transmission Loss for the composite panel: Reference bare layered panel (- - -), metamaterial with NS inclusions (–) having a 30 mm periodicity, panel with a mass-equivalent polyvinyl butyral (PVB) layer inclusion (· · ·).

It is evident that the NS inclusions induce a major improvement of the insulation properties of the panel around its coincidence frequency range (where the acoustic wavenumber becomes equal to the structural one, implying efficient acoustic transmission and a pronounced drop of TL) with a maximum TL increase of about 20 dB. In the high frequency range the advantages are also evident with a constant TL improvement of about 5 dB. On the other hand, in the (mass and stiffness controlled) sub-coincidence range, despite the fact that the loss factor of the layered metamaterial was massively greater, the average TL improvement was inferior to 2 dB. This further confirms the difficulty of increasing noise insulation in the very low frequency range without significant mass addition to the structural panel. It is worth noting that the proposed configuration has outperformed the PVB constrained damping layer in a broadband frequency range, implying not only superior vibration attenuation performance in the low frequency range (due to its considerably greater loss factor) but also better acoustic insulation properties.

4. Conclusions

The principal outcomes of the work are summarised as follows:

(i) The design of mechanical oscillators exhibiting NS behaviour around their snap-through position was discussed. A design appropriate for implementation within a honeycomb structural core was presented and a parametric survey was performed in order to determine the design parameters having a notable impact on its mechanical characteristics. It was demonstrated that an increase of the prestress as well as an increase of the inner radius of the tripod structure can be beneficial for extending the NS region of the device. On the other hand, restricting the rotation of the device at its interface with the core can be detrimental for the NS performance.

(ii) An equivalent FE model of a layered composite metamaterial comprising NS inclusions was presented. A two-dimensional wave scheme for periodic structures was adopted and modified in order to derive an expression for the panel's damping loss factor under the passage of each propagating wave.

(iii) A radical increase of several orders of magnitude was exhibited for the damping ratio of the flexural waves propagating within the suggested structure, particularly in the low frequency range. Comparison with an equivalent structure comprising a constrained damping layer showed that the suggested configuration is highly superior for lower frequencies and performs no worse that the viscoelastic damping layer, even in the post-coincidence frequency range.

(iv) It was shown that the enhanced damping properties of the suggested metamaterial can lead to radical enhancement of its noise insulation properties in the mid and high frequency ranges, while in the very low acoustic frequency range it proves challenging to design an efficiently isolating panel without considerable added mass.

References

[1] M.I. Hussein, M.J. Leamy, M. Ruzzene, Dynamics of phononic materials and structures: Historical origins, recent progress, and future outlook, Appl. Mech. Rev. 66 (2014) 04080–04082.
[2] W. Molyneaux, Supports for vibration isolation, ARC/CP-322, Aeronautical Research Council, Great Britain, 1957.
[3] P. Alabuzhev, E.I. Rivin, Vibration Protection and Measuring Systems with Quasi-Zero Stiffness, CRC Press, 1989.
[4] D.L. Platus, Negative-stiffness-mechanism vibration isolation systems, in: SPIE's International Symposium on Optical Science, Engineering, and Instrumentation, 1999 pp. 98–105.
[5] R. Lakes, Extreme damping in composite materials with a negative stiffness phase, Phys. Rev. Lett. 86 (2001) 2897–2898.
[6] J. Winterflood, D. Blair, B. Slagmolen, High performance vibration isolation using springs in euler column buckling mode, Phys. Lett. A 300 (2002) 122–130.
[7] L. Virgin, R. Davis, Vibration isolation using buckled struts, J. Sound Vib. 260 (2003) 965–973.
[8] R. Plaut, J. Sidbury, L. Virgin, Analysis of buckled and pre-bent fixed-end columns used as vibration isolators, J. Sound Vib. 283 (2005) 1216–1228.
[9] R. DeSalvo, Passive, nonlinear, mechanical structures for seismic attenuation, J. Comput. Nonlinear Dyn. 2 (2007) 290–298.
[10] A. Carrella, M. Brennan, T. Waters, Static analysis of a passive vibration isolator with quasi-zero-stiffness characteristic, J. Sound Vib. 301 (2007) 678–689.
[11] L. Virgin, S. Santillan, R. Plaut, Vibration isolation using extreme geometric nonlinearity, J. Sound Vib. 315 (2008) 721–731.
[12] L. Dong, R. Lakes, Advanced damper with negative structural stiffness elements, Smart Mater. Struct. 21 (2012).
[13] L. Dong, R. Lakes, Advanced damper with high stiffness and high hysteresis damping based on negative structural stiffness, Int. J. Solids Struct. 50 (2013) 2416–2423.
[14] H. Kalathur, R. Lakes, Column dampers with negative stiffness: High damping at small amplitude, Smart Mater. Struct. 22 (2013).
[15] T. Klatt, M.R. Haberman, A nonlinear negative stiffness metamaterial unit cell and small-on-large multiscale material model, J. Appl. Phys. 114 (2013) 033503.
[16] B.A. Fulcher, D.W. Shahan, M.R. Haberman, C.C. Seepersad, P.S. Wilson, Analytical and experimental investigation of buckled beams as negative stiffness elements for passive vibration and shock isolation systems, J. Vib. Acoust. 136 (2014) 03100–03109.
[17] Y. Zhu, Q. Li, D. Xu, C. Hu, M. Zhang, Modeling and analysis of a negative stiffness magnetic suspension vibration isolator with experimental investigations, Rev. Sci. Instrum. 83 (2012).
[18] X. Qu, G. Hou, H. Liu, H. He, Characteristics analysis of the automobile with negative stiffness suspension, Appl. Mech. Mater. 456 (2014) 189–192.
[19] T. Le, K. Ahn, A vibration isolation system in low frequency excitation region using negative stiffness structure for vehicle seat, J. Sound Vib. 330 (2011) 6311–6335.
[20] T. Le, K. Ahn, Experimental investigation of a vibration isolation system using negative stiffness structure, Int. J. Mech. Sci. 70 (2013) 99–112.
[21] L. Danh, K. Ahn, Active pneumatic vibration isolation system using negative stiffness structures for a vehicle seat, J. Sound Vib. 333 (2014) 1245–1268.
[22] C.-M. Lee, V. Goverdovskiy, A multi-stage high-speed railroad vibration isolation system with "negative" stiffness, J. Sound Vib. 331 (2012) 914–921.
[23] H. Iemura, A. Toyooka, M. Higuchi, O. Kouchiyama, Development of negative stiffness dampers for seismic protection, Appl. Mech. Mater. 82 (2011) 645–650.
[24] N. Attary, M. Symans, S. Nagarajaiah, A. Reinhorn, M. Constantinou, A. Sarlis, D. Pasala, D. Taylor, Performance evaluation of negative stiffness devices for seismic response control of bridge structures via experimental shake table tests, J. Earthquake Eng. 19 (2015) 249–276.
[25] D. Pasala, A. Sarlis, A. Reinhorn, S. Nagarajaiah, M. Constantinou, D. Taylor, Apparent weakening in sdof yielding structures using a negative stiffness device: Experimental and analytical study, J. Struct. Eng. (United States) 141 (2015).
[26] W. Gong, S. Xiong, Probabilistic seismic risk assessment of modified pseudo-negative stiffness control of a base-isolated building, Struct. Infrastruct. Eng. (2015) 1–15.
[27] Q. Li, Y. Zhu, D. Xu, J. Hu, W. Min, L. Pang, A negative stiffness vibration isolator using magnetic spring combined with rubber membrane, J. Mech. Sci. Technol. 27 (2013) 813–824.
[28] W. Wu, X. Chen, Y. Shan, Analysis and experiment of a vibration isolator using a novel magnetic spring with negative stiffness, J. Sound Vib. 333 (2014) 2958–2970.
[29] Y. Zheng, X. Zhang, Y. Luo, B. Yan, C. Ma, Design and experiment of a high-static-low-dynamic stiffness isolator using a negative stiffness magnetic spring, J. Sound Vib. 360 (2016) 31–52.
[30] J. Yang, S. Sun, H. Du, W. Li, G. Alici, H. Deng, A novel magnetorheological elastomer isolator with negative changing stiffness for vibration reduction, Smart Mater. Struct. 23 (2014).

[31] S. Sun, J. Yang, H. Deng, H. Du, W. Li, G. Alici, M. Nakano, Horizontal vibration reduction of a seat suspension using negative changing stiffness magnetorheological elastomer isolators, Int. J. Veh. Des. 68 (2015) 104–118.
[32] X. Shi, S. Zhu, Magnetic negative stiffness dampers, Smart Mater. Struct. 24 (2015).
[33] D. Chronopoulos, I. Antoniadis, M. Collet, M. Ichchou, Enhancement of wave damping within metamaterials having embedded negative stiffness inclusions, Wave Motion 58 (2015) 165–179.
[34] R. Langley, A note on the force boundary conditions for two-dimensional periodic structures with corner freedoms, J. Sound Vib. 167 (1993) 377–381.
[35] P. Shorter, Wave propagation and damping in linear viscoelastic laminates, J. Acoust. Soc. Am. 115 (2004) 1917–1925.
[36] E. Manconi, S. Sorokin, On the effect of damping on dispersion curves in plates, Int. J. Solids Struct. 50 (2013) 1966–1973.
[37] V. Cotoni, R. Langley, P. Shorter, A statistical energy analysis subsystem formulation using finite element and periodic structure theory, J. Sound Vib. 318 (2008) 1077–1108.
[38] D. Chronopoulos, M. Ichchou, B. Troclet, O. Bareille, Computing the broadband vibroacoustic response of arbitrarily thick layered panels by a wave finite element approach, Appl. Acoust. 77 (2014) 89–98.